Journal of Computational Physics 322 (2016) 473–490

Contents lists available at ScienceDirect

Journal of Computational Physics

www.elsevier.com/locate/jcp

Accelerating the shifted Laplace preconditioner for the Helmholtz equation by multilevel deflation

A.H. Sheikh [a], D. Lahaye [a,*], L. Garcia Ramos [b], R. Nabben [b], C. Vuik [a]

[a] DIAM, TU Delft, Mekelweg 4, 2611 CN Delft, The Netherlands
[b] TU Berlin, Institut für Mathematik, MA 3-3, Strasse des 17. Juni 136, D-10623 Berlin, Germany

ARTICLE INFO

Article history:
Received 9 March 2015
Received in revised form 23 May 2016
Accepted 16 June 2016
Available online 29 June 2016

Keywords:
Helmholtz equation
Preconditioning
Shifted Laplacian
Deflation
Multigrid
Multilevel Krylov methods

ABSTRACT

Many important physical phenomena can be described by the Helmholtz equation. We investigate to what extent the convergence of the shifted Laplacian preconditioner for the Helmholtz equation can be accelerated using deflation with multigrid vectors. We therefore present a unified framework for two published algorithms. The first deflates the preconditioned operator and requires no further preconditioning. The second deflates the original operator and combines deflation and preconditioning in a multiplicative fashion. We pursue two scientific contributions. First we show, using a model problem analysis, that both algorithms cluster the eigenvalues. The new and key insight here is that the near-kernel of the coarse grid operator causes a limited set of eigenvalues to shift away from the center of the cluster with a distance proportional to the wave number. This effect is less pronounced in the first algorithmic variant at the expense of a higher computational cost. In the second contribution we quantify for the first time the large amount of reduction in CPU-time that results from the clustering of eigenvalues and the reduction in iteration count. We report to this end on the findings of an implementation in PETSc on two and three-dimensional problems with constant and variable wave number.

1. Introduction

The Helmholtz equation is a fundamental physical model for the propagation and scattering of waves. It appears in various branches of science and engineering. Examples include applications in acoustics, seismics and medical imaging. A finite dimensional model is obtained by discretizing the equation using the finite difference or finite element method. This leads to a linear system of equations with a complex symmetric, non-Hermitian and indefinite coefficient matrix. For the wave-like solutions to be sufficiently well resolved a minimum of 10 points per wave length is required. This restriction is often made more stringent to avoid unphysical pollution errors resulting from the discretization [1]. In real-world applications the system of equations therefore becomes too large to be tackled by direct methods. Iterative solvers should be used instead. Most iterative methods however are known to perform very poorly when applied to the Helmholtz equation. A survey is given in [2]. Ideally, the number of iterations of such a method should be independent or only mildly dependent of the wave number and the number of grid points. The wavenumber is here the main parameter of interest.

* Corresponding author.
E-mail addresses: a.h.sheikh@tudelft.nl (A.H. Sheikh), d.j.p.lahaye@tudelft.nl (D. Lahaye), garcia@math.tu-berlin.de (L. Garcia Ramos), nabben@math.tu-berlin.de (R. Nabben), c.vuik@tudelft.nl (C. Vuik).

http://dx.doi.org/10.1016/j.jcp.2016.06.025
0021-9991/

The development of an efficient solver for the Helmholtz equation has attracted considerable attention over the course of the past decades. An important contribution is the publication of the wave-ray method first published in [3] and later further elaborated in [4]. Alternative techniques are the use of multigrid methods with Krylov smoothers [5], sweeping preconditioners [6], domain decomposition [7,8], adaptive [9] and smoothed aggregation multigrid [10] methods. All these techniques have a limited range of applicability and no standard method exists at the moment.

We focus on the complex shifted Laplacian preconditioners (CSLP). These preconditioners introduce damping and render the preconditioned system easy to solve by e.g. multigrid methods. The eigenvalues of the preconditioned operator however move closer to zero as the wave number increases [11,12]. This causes the number of outer Krylov subspace iterations to increase with the wave number. The CSLP preconditioners were initially proposed in [13]. The idea of adding weight to the diagonal of the ILU preconditioner forms the basis of [14]. The CSLP preconditioners were further developed in [15,16] and later generalized in [17–21]. This lead to a breakthrough in industrial applications [22–24]. For a survey we refer to [25].

In this paper we further develop ideas initially established by Erlangga and Nabben in their recent paper [20]. In this paper the authors propose to deploy a deflation procedure [26–28] to remove the eigenmodes that hamper the fast convergence of the CSLP preconditioner. This strategy originated from a deflation perspective that was motivated by previous work on the convection–diffusion equation. The authors employ a relatively large set of multigrid deflation vectors and resort to a multilevel extension to alleviate the computational burden of the coarse grid solve. On each level a Krylov subspace method accelerates the CSLP preconditioner. Spectral analysis and numerical results in [20] show that this so-called multilevel Krylov method significantly reduces the required number of iterations. The required deflated preconditioned operator is too difficult to construct and some form of approximation is mandatory. Such an approximation results in a computationally feasible multilevel method in [20]. An alternative multilevel Krylov approach in which the original Helmholtz operator is deflated instead was proposed in [29]. This approach circumvents the necessity of constructing expensive operators.

In this paper we give a unified presentation of the methods proposed in [20] and in [29]. The method in [20] deflates the CSLP preconditioned system and requires no further preconditioning. The method published in [29] deflates the Helmholtz operator and combines this deflation multiplicatively with the CSLP preconditioner. Both methods use a flexible Krylov method on each level and can be seen as preconditioned multilevel Krylov methods. We perform a Fourier analysis of the one-dimensional model problem in which the homogeneous Dirichlet boundary conditions are explicitly taken into account. We analyze two-level variants of both algorithms assuming standard coarsening of a uniform mesh and the exact inversion of both the preconditioner and the coarse grid operator. With these assumptions, the Helmholtz operator, the CSLP preconditioned operator and the multigrid deflated preconditioned operator share a set of orthogonal eigenvectors and are thus normal. The convergence theory for GMRES can thus be applied. The analysis shows that both algorithms are governed by a spectrum whose convex hull has a characteristic dimension that grows with the wave number. The key new insight that this paper provides is the link between the shifting of a limited number of eigenvalues away from a common cluster and the shifting towards zero of eigenvalues of the coarse grid operator as the wave number increases. The first algorithm provides a better clustering at the expenses of a substantially higher computational cost.

We implemented the second method within the PETSc [30] software library. We tested this code on two- and three-dimensional test problems with constant and variable wave numbers. These problems were discretized by a second order finite difference scheme on increasingly finer meshes. The numerical results show that the use of deflation results in a reduction in iteration count. This reduction grows with the wave number. It thus confirms the spectral analysis that predicts that the use of deflation results in a more favorable eigenvalue distribution. The reduction in iterations results in a significant reduction in CPU time for sufficiently large problems. The numerical results for the non-constant wavenumber problems show that the method does work for such problems as well. On the three-dimensional test cases considered the use of deflation results in speedup of a factor between six and ten.

This paper is structured as follows: In Section 2 we describe the model problems, their finite difference discretization and the eigenvalues of the discrete Helmholtz operator. In Section 3 we describe the CSLP preconditioner and give the eigenvalues of the preconditioned operator. In Section 4 we introduce the framework for multilevel deflation methods. In Section 5 and Section 6 we conduct a model problem analysis for the first and second solution algorithm, respectively. In Section 7 we show numerical results. Finally we draw conclusions in Section 8.

2. Problem formulation

On the computational domain Ω with boundary $\partial\Omega$ and outward normal n we consider the Helmholtz equation for the unknown field $u(\mathbf{x})$

$$-\Delta u(\mathbf{x}) - (1-\alpha\imath)k^2(\mathbf{x})u(\mathbf{x}) = g(\mathbf{x}), \tag{2.1}$$

where $\imath$, α, $k(\mathbf{x})$ and $g(\mathbf{x})$ are the imaginary unit, the damping parameter, the wave number and the source function, respectively. The wave number $k(\mathbf{x})$, the frequency f and angular frequency $\omega = 2\pi f$, the speed of propagation $c(\mathbf{x})$ and the wave length $\lambda = \frac{c(\mathbf{x})}{f}$ are related by

$$k = \frac{2\pi}{\lambda} = \frac{\omega}{c(\mathbf{x})}. \tag{2.2}$$

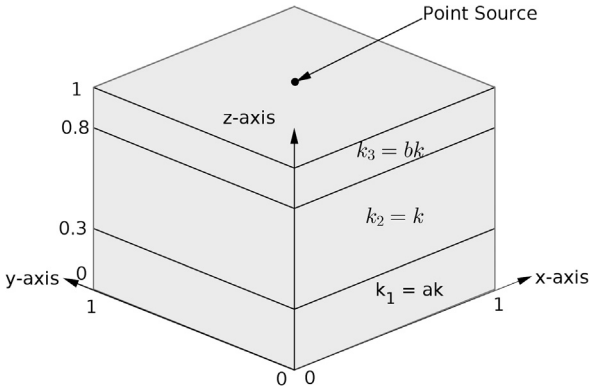

Fig. 1. Layered wave number distribution and point source location in three dimensional unit cube domain.

On the boundary $\partial\Omega$ we impose the homogeneous first order Sommerfeld radiation boundary condition given by

$$\frac{\partial u}{\partial n} - \iota k u = 0 \text{ on } \partial\Omega\,. \tag{2.3}$$

In the analysis of the solvers we will make use of homogeneous Dirichlet boundary conditions. To demonstrate the performance of the solver by numerical experiments, we will make use of the following three model problems.

Problem 1. The first problem is posed on the unit cube $\Omega = (0,1)^3$. The wave number k is assumed to be constant on Ω. The damping parameter α is set equal to zero. The source function $g(\mathbf{x})$ is modeled as a Dirac delta function centered in the Centre of the domain

$$g(x_1, x_2, x_3) = \delta(x_1 - \frac{1}{2}, x_2 - \frac{1}{2}, x_3 - \frac{1}{2})\,. \tag{2.4}$$

Problem 2. The second problem is posed on the unit cube $\Omega = (0,1)^3$ subdivided into three layers parallel to the x_1x_2-plane as shown in Fig. 1. In this figure the x_3-axis points upward. The wave number is assumed to be constant on each layer and its value in the top and bottom layer is assumed to be equal to $a = 1.2$ and $b = 1.5$ times the value in the middle layer, respectively. Damping is set equal to zero as in the previous problem. The excitation is caused by a point source located in the middle of the top surface where $x_3 = 1$, i.e.,

$$g(x_1, x_2, x_3) = \delta(x_1 - \frac{1}{2}, x_2 - \frac{1}{2}, x_3 - 1)\,. \tag{2.5}$$

Problem 3. The third problem is a modified Marmousi problem [31] in which the original computational domain $\Omega = (0, 3000\,\text{m}) \times (0, 9200\,\text{m})$ was reduced to $\Omega = (0, 2048\,\text{m}) \times (0, 8192\,\text{m})$. This reduction allows a convenient geometrical coarsening of a uniform fine mesh by reducing the mesh size by a factor of two in each direction. The contrast in the wave number was reduced by limiting the range of the speed of propagation $c(\mathbf{x})$ to $2587.5\,\text{m/s} \le c(\mathbf{x}) \le 3325\,\text{m/s}$. The geometric multigrid method used to approximately invert the complex shifted Laplace preconditioner appears not to be robust for higher contrast values. In the future we will investigate and implement more advanced multigrid methods. Here both the cases of no and small damping will be considered. This problem will be solved using the frequencies $f = 1,\ 10,\ 20$ and $40\,\text{Hz}$. A point source is centered in $x_1 = 1024\,\text{m}$ and $x_2 = 0$.

Finite difference discretization. The finite difference discretization of two-dimensional problems on a uniform mesh with mesh width h in both directions with stencil

$$[A_h] = \frac{1}{h^2}\begin{bmatrix} 0 & -1 & 0 \\ -1 & 4-(1-\alpha\iota)\kappa^2 & -1 \\ 0 & -1 & 0 \end{bmatrix} \text{ where } \kappa = k\,h\,, \tag{2.6}$$

leads to a system of linear equations

$$A_h x_h = b_h, \tag{2.7}$$

where the discrete Helmholtz operator A_h is the sum of the finite difference discretized Laplacian $-\Delta_h$ and $-k^2$ times the identity I_h

$$A_h = -\Delta_h - (1-\alpha\iota)k^2 I_h\,. \tag{2.8}$$

Stencil (2.6) is easily adapted to one and three-dimensional problems. The point sources are treated in a finite difference setting by setting the i-th component of the right-hand side vector g equal to $g(i) = 1/h^d$, where i and d are the index corresponding to the source in the global enumeration of the grid nodes and the dimension of the problem, respectively. The treatment of the first order Sommerfeld boundary condition (2.3) adds a term $\imath k u$ to the diagonal. The discretized operator remains complex symmetric. The numerical representation of waves requires the grid to be sufficiently fine. This is especially true in cases in which the computational domain contains many wave lengths. We will enforce the use of a fixed number of nodes per wave length [32]. The use of at least 10 nodes per wave length for instance leads to the restriction

$$\kappa \leq \frac{2\pi}{10} \approx 0.628\,. \tag{2.9}$$

In problems in which the wave number is constant per subdomain (as in Problem 2 and Problem 3), the discontinuity in wavenumber is allowed to cut through the finite difference grid cells. As the contrast in the wavenumber is relatively small (ratio less than three), no special adaptions to the discretization scheme are made. The largest wave number is then used to enforce condition (2.9). For a discussion on higher order finite difference approximations for the Helmholtz equation, we refer to e.g. [33].

Spectral analysis. The linear system matrix A_h is sparse, symmetric, indefinite and has in the absence of damping a non-empty near-null space. In this paragraph we will discuss the spectrum of A_h. The information provided here will be used as a reference to study the spectrum of the CSLP preconditioned and deflated operator in the forthcoming sections. We will employ a sequence of coarser levels to solve the linear system (2.7) for various values of k. We will study how the spectrum of A_h changes as k increases while κ is kept fixed.

The discretization of the one-dimensional Helmholtz operator on a uniform mesh with mesh width $h = 1/n$ with Dirichlet boundary conditions results in a matrix of size $A_h \in \mathbb{R}^{(n-1)\times(n-1)}$ assuming that the boundary nodes have been eliminated. In the absence of damping, the eigenvalues of A_h are the negatively shifted eigenvalues of the discrete Poisson operator and are given by [29,2]

$$\lambda^{\ell}(A_h) = \frac{1}{h^2}(2 - 2c_{\ell} - \kappa^2)\,, \tag{2.10}$$

for $1 \leq \ell \leq n-1$, where

$$c_{\ell} = \cos(\ell\,\pi\,h)\,. \tag{2.11}$$

The corresponding eigenvectors are the discrete sine modes. As this set is orthogonal, the matrix A_h is normal. The use of Dirichlet boundary conditions renders the boundary of the computational domain reflective for outgoing waves. One could instead consider problems in which (part of) the boundary is transparent for outgoing waves through the use of absorbing boundary conditions. Results in e.g. [15,11] indicate that for these boundary conditions the discrete operators have a more favorable spectrum for Krylov methods. In the following we will scale the eigenvalues $\lambda^{\ell}(A_h)$ with h^2. This scaling cancels the h^2 in the denominator of (2.10). This canceling will naturally arise in the forthcoming spectral analysis of the preconditioned and the deflated operator.

The near-null space of $h^2\,A_h$ will play a very important role in the analysis. The null-space of $h^2\,A_h$ is defined by the index ℓ^* such that $\lambda^{\ell^*}(h^2\,A_h) = 2 - 2c_{\ell^*} - \kappa^2$ is minimal, or equivalently

$$\ell^* = \text{round}\left[\frac{1}{\pi h}\arccos(1 - \kappa^2/2)\right]. \tag{2.12}$$

For a fixed value of k, this value of ℓ^* is nearly constant in κ in the range of κ considered. This implies that for fixed k, the null space of $h^2\,A_h$ shift towards lower frequencies as the number of grid points per wavelength is increased. The near-null space of $h^2\,A_h$ is defined as the set of those values of ℓ for which $\lambda^{\ell}(h^2\,A_h)$ is smaller than some tolerance.

In Fig. 2 we plotted the eigenvalues of $h^2\,A_h$ for two values of the wavenumber, namely $k = 100$ and $k = 10{,}000$ and for each of these values using both 10 and 20 grid points per wavelength. On the x-axis we labeled the value of ℓ^* computed using $\kappa = 0.625$ and equal to $\ell^* = 32$ and $\ell^* = 3237$ for $k = 100$ and $k = 10{,}000$, respectively. The range on the y-axis is bounded below by $-\kappa^2$ (where $c_{\ell=1} \approx 1$) and above by $4 - \kappa^2$ (where $c_{\ell=n-1} \approx -1$). We will use values as large as $k = 10{,}000$ to illustrate features of our analysis that appear in the limit of large k.

In Fig. 3 we plotted on the left the smallest eigenvalue $\lambda^{\ell^*}(h^2\,A_h)$ as a function of the wavenumber k in the range between $k = 0$ and $k = 1000$ using both 10 and 20 grid points per wavelength. The value of $\lambda^{\ell^*}(h^2\,A_h)$ is seen to converge to zero, although non-monotonically. On the right we plotted the number of small eigenvalues again for 10 and 20 grid points per wavelength in the same range k as before. Fig. 3 confirms earlier statements made on $\lambda^{\ell^*}(h^2\,A_h)$ and the near-kernel of A_h.

We conclude this section by summarizing the most salient features of the spectral analysis of the scaled discrete Helmholtz operator $h^2\,A_h$. We saw that increasing k while κ is kept constant has the following two important consequences:

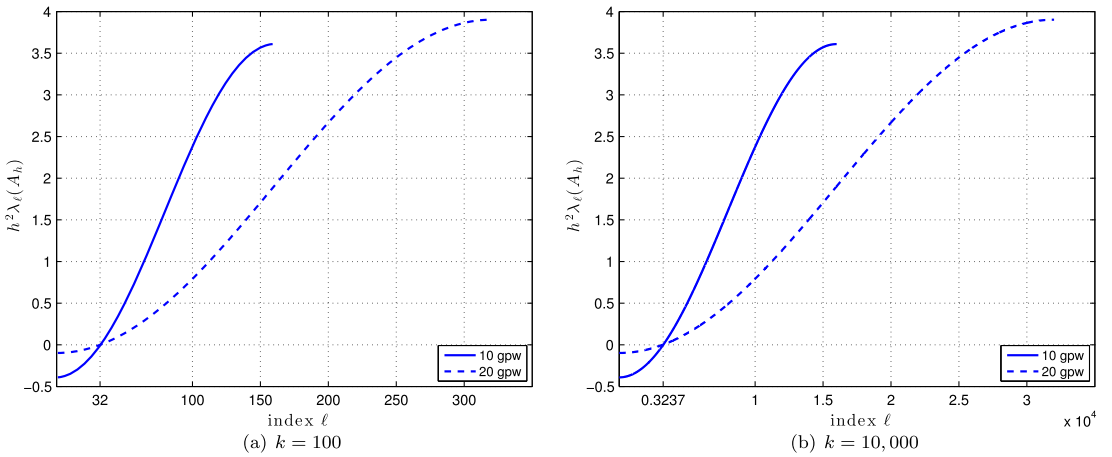

Fig. 2. Eigenvalues of the h^2-scaled 1D Helmholtz operator A_h with Dirichlet boundary conditions for $k = 100$ and $k = 10{,}000$ using both 10 (solid line) and 20 (dashed line) grid points per wavelength.

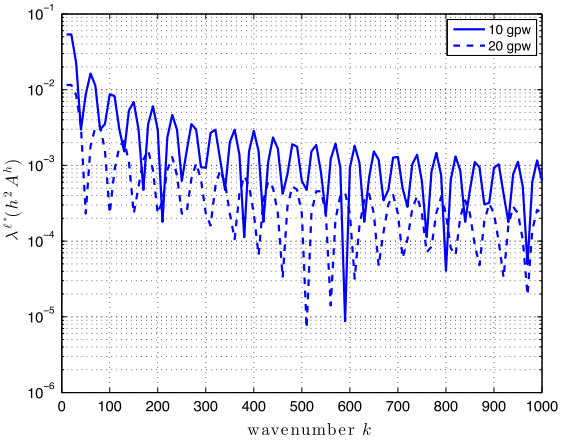

Fig. 3. Size of smallest eigenvalue of h^2A^h as a function of the wavenumber for both 10 (solid line) and 20 (dashed line) grid points per wavelength.

- the smallest eigenvalue becomes smaller due to finer grid resolution;
- the number of eigenvalues in the near-kernel relative to the problem size increases.

Decreasing instead κ while k is kept constant (by increasing the number of grid points) has the consequences that

- the near-kernel shift towards the lower end of the spectrum;

These consequences will be key aspects in explaining the spectrum of the CSLP preconditioned and deflated Helmholtz operator in the forthcoming sections.

3. Shifted Laplacian preconditioner

The complex shifted Laplace (CSLP) preconditioner [13,15] is currently ranked among the most efficient preconditioners for the Helmholtz equation. Denoting by β_2 the damping parameter, this preconditioner can be written as[1]

$$M_{h,\beta_2} = -\Delta_h - (1 + \imath\,\beta_2)\,k^2 I_h \text{ with } \beta_2 \in \mathbb{R}\,. \tag{3.1}$$

In this paper we will consider both left and right preconditioning. The CSLP preconditioners are effective because they transform the spectrum of A_h into the spectrum of $A_h M_{h,\beta_2}^{-1}$ that lies in the right half of the complex plane and that is mostly clustered around $(1, 0)$. For such spectra, the Krylov methods converge faster than for the spectra of the Helmholtz operator

[1] To be consistent with the notation previously introduced in e.g. [34], we denote the damping parameter in the CSLP preconditioner by β_2 and set the parameter β_1 introduced in [34] equal to one.

as extensively shown both by theory and experiments in e.g. [15,16,11,17–19]. The term with β_2 introduces damping in the preconditioner and renders the solution of a linear system with M_{h,β_2} as coefficient matrix easy to compute. In the literature, approximate inversions using either MILU [14], geometric [20,34] or algebraic multigrid [19,18] have been studied. In this work we will use geometric multigrid with Galerkin coarsening on a sequence of uniformly coarsened meshes.

The amount of damping (i.e. the value of β_2) needs to balance the quality of the preconditioner (favoring small damping) with the ease to invert it (favoring large damping). This balance has received considerable attention in the literature [16,11, 17,29,21]. The results of the recent paper [21] indicate that the complex shift in (3.1) should scale like the wave number k in order to obtain an optimal preconditioner for the Helmholtz operator. Results in the paper [29] instead indicate that the combined use of the CSLP preconditioner allows to increase the amount of damping without compromising the convergence of the outer Krylov iteration. This motivates the choice of $\beta_2 = 1$ and $\beta_2 = .5$ in this paper when used with and without deflation, respectively.

Spectral analysis. Paper [11] analyzes the spectrum of the shifted Laplace preconditioned Helmholtz operator $A_h M_{h,\beta_2}^{-1}$ in detail. This analysis shows that eigenvalues of the preconditioned system lie in a circle with radius 0.5 centered in $(0.5, 0)$. These eigenvalues shift towards zero as the wave number increases. This explains the non-scalability of the CSLP preconditioner with increasing wave number. In this paragraph we show that the eigenvalues shifting to zero are those corresponding to the near-null space of $h^2 A_h$. This motivates the use of deflation to remove these small eigenvalues. We consider to this end again the one-dimensional problem without damping and with Dirichlet boundary conditions discretized on a uniform mesh with mesh width $h = 1/n$. In case that the preconditioner is inverted exactly, A_h and M_{h,β_2}^{-1} share a basis of orthogonal eigenvectors. The matrices $A_h M_{h,\beta_2}^{-1}$ and $M_{h,\beta_2}^{-1} A_h$ are then similar and normal. We expect that the similar results carry over to higher dimensional problems that include damping or other boundary conditions.

Given the above assumptions, the eigenvalues of M_{h,β_2} for $1 \leq \ell \leq n-1$ are given by

$$\lambda^\ell(h^2 M_{h,\beta_2}) = \lambda^\ell(h^2 A_h) - \iota\beta_2\kappa^2\,, \tag{3.2}$$

where $\lambda^\ell(h^2 A_h)$ is given by (2.10). The eigenvalues of $A_h M_{h,\beta_2}^{-1}$ for $1 \leq \ell \leq n-1$ are thus given by

$$\begin{aligned}\lambda^\ell(A_h M_{h,\beta_2}^{-1}) &= \frac{\lambda^\ell(h^2 A_h)}{\lambda^\ell(h^2 A_h) - \iota\beta_2\kappa^2} \\ &= \frac{\left[\lambda^\ell(h^2 A_h)\right]^2}{\left[\lambda^\ell(h^2 A_h)\right]^2 + \beta_2^2\kappa^4} + \iota\frac{\lambda^\ell(h^2 A_h)\beta_2\kappa^2}{\left[\lambda^\ell(h^2 A_h)\right]^2 + \beta_2^2\kappa^4}\end{aligned} \tag{3.3}$$

The real and imaginary part of $\lambda^\ell(A_h M_{h,\beta_2}^{-1})$ are thus small in size for those values of ℓ for which $\lambda^\ell(h^2 A_h)$ is small. We more precisely have that

$$\begin{aligned}\ell^* = \text{argmin}_{1\leq\ell\leq n-1}\left|\lambda^\ell(h^2 A_h)\right| &= \text{argmin}_{1\leq\ell\leq n-1}\text{Re}\left[\lambda^\ell(A_h M_{h,\beta_2}^{-1})\right] \\ &= \text{argmin}_{1\leq\ell\leq n-1}\text{Im}\left[\lambda^\ell(A_h M_{h,\beta_2}^{-1})\right]\end{aligned} \tag{3.4}$$

From the discussion in the previous section we can then infer that increasing k while κ is kept constant has the following two important consequences. The first is that the smallest real and imaginary part of $A_h M_{h,\beta_2}^{-1}$ becomes smaller. The second is that the number of eigenvalues small in size increases. For eigenvalues in the near-kernel of $h^2 A^h$ we can set $\epsilon = \lambda^\ell(h^2 A_h) \ll 1$. Clearly ϵ is a function of both k and h. The real and imaginary part of $A_h M_{h,\beta_2}^{-1}$ can then for small ϵ be written as

$$\begin{aligned}\text{Re}\left[\lambda^\ell(A_h M_{h,\beta_2}^{-1})\right] &= \frac{\epsilon^2}{\epsilon^2 + \beta_2^2\kappa^4} = \frac{2}{\beta_2^2\kappa^4}\epsilon^2 + \mathcal{O}(\epsilon^3)\,, \\ \text{Im}\left[\lambda^\ell(A_h M_{h,\beta_2}^{-1})\right] &= \frac{\beta_2\kappa^2\epsilon}{\epsilon^2 + \beta_2^2\kappa^4} = \frac{1}{\beta_2\kappa^2}\epsilon + \mathcal{O}(\epsilon^2)\,.\end{aligned} \tag{3.5}$$

The action of the preconditioner is seen to map the near-kernel eigenvalues ϵ of A_h to near-kernel eigenvalues eigenvalues $(\frac{2}{\beta_2^2\kappa^4}\epsilon^2, \frac{1}{\beta_2\kappa^2}\epsilon)$ of $A_h M_{h,\beta_2}^{-1}$. Given that for a fixed value of k and h holds that $\beta_2\kappa^2 \ll 1$, the popularity of the CSLP preconditioner can be explained by the relative increase of the imaginary part of the smallest eigenvalue.

The CSLP preconditioner does however require more iterations as k increases while κ is held constant and is therefore not scalable. This can be explained by the smallest eigenvalue of $A_h M_{h,\beta_2}^{-1}$ to become smaller and the number of small eigenvalues to increase. The number of unfavorable eigenvalues however remains limited and decreases as κ is decreased. This motivates looking into the use of deflation to remove them from the spectrum of the preconditioned matrix.

4. Multilevel deflation

In this section we describe the multilevel deflation method. We subsequently discuss the two-level deflation method, its combination with a preconditioner and its multilevel extension. In the next section we give more details on the application of these ideas to the discretized Helmholtz equation.

The convergence of the CSLP preconditioned Krylov methods for the Helmholtz equation is hampered by small eigenvalues. As the wavenumber k increases while κ is held fixed, the smallest eigenvalue decreases in size and the number of small eigenvalues increases. Deflation is a technique that aims at dealing with these small eigenvalues [28,26,27]. The basic idea is to bring the small eigenvalues to zero by a projection procedure.

Two-level deflation. Here we briefly explain the two-level deflation technique to solve the linear system resulting from the discretization of a PDE on a fine mesh with grid size h

$$A_h x_h = b_h\,. \tag{4.1}$$

We assume a coarse mesh with grid size H to be also available and denote by $Z_{h,H}$ the interpolation operator mapping from the coarse to the fine mesh. Later, we assume the fine mesh to be uniform, the coarse mesh to be constructed geometrically by standard coarsening and the interpolation to be linear in each coordinate direction. The columns of $Z_{h,H}$ are referred to as the multigrid vectors. We use Galerkin coarsening to construct the coarse grid operator

$$E_H = Z_{h,H}^T A_h Z_{h,H} \tag{4.2}$$

and denote the coarse grid solve matrix as $Q_{h,H} = Z_{h,H} E_H^{-1} Z_{h,H}^T$. The deflation operator $P_{h,H}$ is then defined as

$$P_{h,H} = I_h - A_h Q_{h,H}\,. \tag{4.3}$$

This operator corresponds with the residual propagation operator in a coarse grid correction scheme. It satisfies the relation $(P_{h,H})^2 = P_{h,H}$ and thus defines a projection. Each column of $Z_{h,H}$ belongs to the kernel of the deflated operator $P_{h,H}A_h$. The spectrum of $P_{h,H}A_h$ therefore contains zero as an eigenvalue [28]. In case that E_H is inverted only approximately, the projection property is lost and eigenvalues close to zero in the spectrum of $P_{h,H}A_h$ appear [26]. By applying the deflation operator, system (4.1) is transformed into

$$P_{h,H} A_h \tilde{x}_h = P_{h,H}\, b_h\,, \tag{4.4}$$

which can be solved by a Krylov subspace method. To obtain a unique solution of (4.1) the computed $\tilde{x}_h$ must be updated by

$$x_h = (I_h - Q_{h,H}\, A_h)\, \tilde{x}_h + Q_{h,H}\, b. \tag{4.5}$$

We call this technique *two-level deflation*. The geometric construction of the deflation vectors is such that the number of deflation vectors increases with the wave number and the dimensions of the problem. This construction is in accordance with the increase of small eigenvalues with these parameters. This technique can be extended to higher order discretization methods by using the columns of the interpolation operator proposed in [33] as deflation vectors.

The two-level deflation technique can be combined with a preconditioner M_h in two ways that we will refer as *First Precondition, then Deflate* and *First Deflate, then Preconditioning* in the following two paragraphs.

First Precondition, then Deflate. To combine the two-level deflation technique with preconditioning, one can deflate the preconditioned operator and avoid any subsequent application of the preconditioner. This approach is motivated by two previous papers [35,36] that show that diagonal scaling prior to deflating the discretized convection–diffusion operator results in a tight clustering of eigenvalues. Preconditioning from the right transforms the linear system (4.1) into

$$\widehat{A}_h \hat{x}_h = b_h \text{ where } \widehat{A}_h = A_h M_h^{-1} \text{ and } \hat{x}_h = M_h x_h\,. \tag{4.6}$$

Deflating this linear system requires in the Galerkin operator

$$\widehat{E}_h = Z_{h,H}^T \widehat{A}_h Z_{h,H}\,, \tag{4.7}$$

the coarse grid solve operator $\widehat{Q}_{h,H} = Z_{h,H} \widehat{E}_H^{-1} Z_{h,H}^T$ and the deflation operator

$$\widehat{P}_{h,H} = I_h - \widehat{A}_h \widehat{Q}_{h,H}\,. \tag{4.8}$$

As before we have that $(\widehat{P}_{h,H})^2 = \widehat{P}_{h,H}$. This variant then solves the deflated linear system

$$\widehat{P}_{h,H} \widehat{A}_h \tilde{x}_h = \widehat{P}_{h,H} b_h\,, \tag{4.9}$$

and no additional form of preconditioning is used. This method is referred to as the Multilevel Krylov method (MK-method) and if the CSLP preconditioner is used as the MKMG-method in [35,36].

This method requires the explicit construction of $\widehat{E}_H = Z_{h,H}^T A_h M_h^{-1} Z_{h,H}$. This construction is feasible if the preconditioner is sufficiently simple to apply. An example is the use of diagonal scaling as in [35,36]. In case of CSLP preconditioning of the Helmholtz equation however, the preconditioner is much more expensive to apply. A matrix-free approach which the matrix–vector multiplication with the matrix $Z_h^T A_h M_{h,\beta_2}^{-1} Z_h$ is replaced by the action of this matrix on a vector still requires too many fine grid computations and still costs too much work per iteration. Some form of approximation in constructing operator $\widehat{E}_H$ is therefore mandatory. One alternative is to coarsen the preconditioner and the original operator separately, i.e., to build the operators $M_{H,\beta_2} = Z_{h,H}^T M_{h,\beta_2} Z_{h,H}$ and $E_H = Z_{h,H}^T A_h Z_{h,H}$ and to subsequently approximate $\widehat{E}_H$ as

$$\widehat{E}_H = Z_{h,H}^T (A_h M_{h,\beta_2}^{-1}) Z_{h,H} \approx E_H M_{H,\beta_2}^{-1} = \hat{\widehat{E}}_H . \tag{4.10}$$

Let $\hat{\widehat{P}}_{h,H}$ denote the corresponding deflation operator. This approximation is such that the deflation operator defined ceases to satisfy the relation $(\hat{\widehat{P}}_{h,H})^2 = \hat{\widehat{P}}_{h,H}$ and thus ceases to define a projection. The computational feasibility comes at the price of a spectrum that is less favorable to the convergence of the outer Krylov iteration. This is essentially due to the fact that a coarse grid solve by the complex shifted Laplacian $\widehat{E}_H$ is replaced by a coarse grid solve that involves the Helmholtz operator E_H. Details will be given in the next section.

First deflate, then precondition. To combine the two-level deflation technique with preconditioning, one can alternatively deflate the original system matrix and combine the deflation and the preconditioner operators in a multiplicative fashion. The coarse grid operator and deflation operator are then defined by (4.2) and (4.3). If we choose to apply the preconditioner after the deflation, the linear system to be solved can be written as

$$M_{h,\beta_2}^{-1} P_{h,H} A_h \tilde{x} = M_{h,\beta_2}^{-1} P_{h,H} b_h . \tag{4.11}$$

The explicit construction or approximation of $A_h M_{h,\beta_2}^{-1}$ is avoided in this approach.

Multilevel deflation. In a two-level method the coarse grid operators E_H and $\widehat{E}_H$ remain too large in size to be inverted exactly. A multilevel extension is thus needed to become computationally viable. In such an extension the coarse grid solve requires attention in order to avoid close-to-zero eigenvalues in the spectrum of $P_{h,H} A_h$ or $\widehat{P}_{h,H} \widehat{A}_h$. Such small eigenvalues will hamper the convergence of the Krylov method. This can be addressed by adding to $P_{h,H}$ a scalar γ times $Q_{h,H}$ which leads to the operator

$$P_{h,H,\gamma} = P_{h,H} + \gamma Q_{h,H} = I_h - A_h Q_{h,H} + \gamma Q_{h,H} , \tag{4.12}$$

[27] and similarly for $\widehat{P}_{h,H,\gamma}$ and $\hat{\widehat{P}}_{h,H,\gamma}$. The linear system to be solved can now be written as

$$(M_{h,\beta_2}^{-1} P_{h,H} + \gamma Q_{h,H}) A_h \tilde{x} = (M_{h,\beta_2}^{-1} P_{h,H} + \gamma Q_{h,H}) b_h . \tag{4.13}$$

For $\gamma = 1$ this corresponds to a two-grid V(0, 1)-cycle with M_{h,β_2} as a smoother in a multigrid context. This method is referred to as the Adaptive Deflation 1 (A-DEF1) method in [27]. We will refer to the matrix

$$B_{h,H,\beta_2} = (M_{h,\beta_2}^{-1} P_{h,H} + \gamma Q_{h,H}) A_h \tag{4.14}$$

as the preconditioned deflated matrix without and with shift if $\gamma = 0$ and $\gamma \neq 0$, respectively. The term with γ allows to solve the coarser grid system with matrix E_H, $\widehat{E}_H$ or $\hat{\widehat{E}}_H$ inexactly using flexible Krylov subspace solvers preconditioned using a next coarser level. This gives rise to a so-called multilevel Krylov method [35,36]. Numerical experiments in [20] and [29] have shown that solving the first coarser level more accurately than the other levels is beneficial for the convergence of the outer Krylov iteration. An algorithmic representation of the multilevel First Deflate, Then Precondition algorithm is given in Algorithm 1.

Neither $P_{h,H,\gamma}$ nor $\widehat{P}_{h,H,\gamma}$ is a projection. The only difference in the spectrum of $P_{h,H} A_h$ and $P_{h,H,\gamma} A_h$ is that the zero eigenvalue of $P_{h,H} A_h$ is replaced by γ in the spectrum of $P_{h,H,\gamma} A_h$ (and similarly for $\widehat{P}_{h,H,\gamma} \widehat{A}_h$). The term $\gamma Q_{h,H}$ acts like a shift. The parameter γ is in most applications set equal to the largest eigenvalue of the preconditioned operator. As the eigenvalues largest in magnitude of $A_h M_{h,\beta_2}^{-1}$ is bounded by one, we set $\gamma = 1$ in the following. In the theorem that follows, we prove that $P_{h,H,\gamma}$ is nonsingular for $\gamma = 1$.

Theorem 1. *Let $A, M \in \mathbb{C}^{n\times n}$ be nonsingular matrices and $Z \in R^{n\times r}$ of full rank, where $r < n$. Suppose that the Galerkin matrix $Z^T A Z$ is nonsingular and let $Q = Z(Z^T A Z)^{-1} Z$ and $P = M^{-1}(I - A Q) + Q$. Then P is nonsingular if and only if the Galerkin matrix $Z^T M Z$ is nonsingular.*

Proof. Note that $\tilde{P} = I - AQ$ is the projection (i.e. $\tilde{P}^2 = \tilde{P}$) onto $\mathrm{im}(Z)^\perp$ along $\mathrm{im}(AZ)$, therefore $\mathrm{im}(\tilde{P}) = \mathrm{im}(Z)^\perp$ and $\ker(\tilde{P}) = \mathrm{im}(AZ)$. Also, observe that $Q = A^{-1}(I - \tilde{P})$, and since $(I - \tilde{P})$ is the complementary projection of $\tilde{P}$ we have $\mathrm{im}(Q) = \mathrm{im}(Z)$ and $\ker(Q) = \mathrm{im}(Z)^\perp$.

We show first the "⇒" implication. Let $x \in \mathbb{C}^n$ with $Px = 0$. Then $MPx = (I - AQ)x + MQx = 0$, and if $y = (I - AQ)x = -MQx$, we have $y \in \mathrm{im}(\tilde{P}) \cap \mathrm{im}(MQ) = \mathrm{im}(Z)^{\perp} \cap \mathrm{im}(MZ)$. So $y = MZ\hat{y}$ for some $\hat{y} \in \mathbb{C}^r$ and $Z^T y = Z^T MZ\hat{y} = 0$. Since $Z^T MZ$ is nonsingular this implies $\hat{y} = 0$, and also $y = 0$ which gives $x = 0$. Therefore P is nonsingular.

For the implication "⇐", we prove the contrapositive. Suppose that $Z^T MZx = 0$ for some $x \neq 0$. Let $y = MZx$ and $z = AZx$, then $y \neq 0$ and $z \neq 0$ since M and A are nonsingular and Z is full rank. Moreover, $y \in \mathrm{im}(Z)^{\perp}$ and $z \in \mathrm{im}(AZ)$. Let $w = y - z$, we will show that $w \neq 0$ and $Pw = 0$. For the first assertion, suppose that $w = 0$, then $y = z$ and $y \in \mathrm{im}(Z)^{\perp} \cap \mathrm{im}(AZ)$, but since $\mathrm{im}(Z)^{\perp} \cap \mathrm{im}(AZ) = \{0\}$ because the projection $\tilde{P}$ is well defined (cf. the remark at the beginning of the proof) this gives $y = 0$ which is not possible. Hence $w \neq 0$. The equality $Pw = 0$ follows from a direct computation that can be simplified recalling the projection representations mentioned at the beginning of the proof:

$$\begin{aligned} Pw &= (I - AQ)(y - z) + Q(y - z) \\ &= \tilde{P}(y - z) + A^{-1}(I - \tilde{P})(y - z) \\ &= y - A^{-1}z \\ &= Zx - Zx = 0. \end{aligned}$$

Remark 1. This theorem proves that the matrix $P_{h,H,\gamma}$ defined by (4.12) in the First Deflate, Then Precondition Method is non-singular for $\gamma = 1$. The theorem with A replaced by $\widehat{A} = M^{-1}A$ and $M = I$ proves that the matrix $\widehat{P}_{h,H,\gamma}$ defined in the First Precondition, Then Deflate Method is non-singular for $\gamma = 1$.

Algorithm 1 The First Deflate, Then Precondition (A-DEF1) method including the shift on multiple levels used as a preconditioner for a flexible Krylov subspace. The coarse grid problem is solved by the same Krylov subspace method preconditioned again by the First Deflate, Then Precondition method.

Solve $A_h x_h = b_h$ by a Flexible Krylov method preconditioned by the following three-step multiplicative procedure that given the residual r_h^i at iteration i computes the new search direction z_h^{i+1}

1	$z_h^{i+1/3} = P_{h,H} r_h^i$	Deflation without shift
	1.1: $r_H^i = Z_{h,H}^T r_h^i$	Restrict to coarse grid
	1.2: $e_H^i = E_H^{-1} r_H^i$	Coarse grid solve by recursion
	1.3: $s_h^i = Z_{h,H} e_H^i$	Interpolate to fine grid Therefore $s_h^i = Q_{h,H} r_h^i$
	1.4: $t_h^i = A_h s_h^i$	Matrix–vector multiply Therefore $t_h^i = A_h Q_{h,H} r_h^i$
	1.5: $z_h^{i+1/3} = r_h^i - t_h^i$	Adding intermediate results Therefore $z_h^{i+1/3} = P_{h,H} r_h^i$
2	$z_h^{i+2/3} = M_{h,\beta_2}^{-1} z_h^{i+1/3}$	CSLP Preconditioning Therefore $z_h^{i+2/3} = M_{h,\beta_2}^{-1} P_{h,H} r_h^i$
3	$z_h^{i+1} = z_h^{i+2/3} + s_h^i$	Adding the shift Therefore $z_h^{i+1} = (M_{h,\beta_2}^{-1} P_{h,H} + Q_{h,H}) r_h^i$

5. Model problem analysis of first precondition, then deflate

In this section we perform a spectral analysis of the First Precondition, Then Deflate method introduced in the previous section. We will study both variants that use the matrices $\widehat{E}_H$ and $\hat{\widehat{E}}_H$ defined by (4.7) and (4.10) as coarse grid matrices, respectively. For the variant that uses $\widehat{E}_H$, we will derive analytical expressions for the eigenvalues of the deflated preconditioned Helmholtz operator that we will denote as

$$\widehat{B}_{h,H,\beta_2} = \widehat{P}_{h,H}\,\widehat{A}_h = \widehat{P}_{h,H}\,A_h\,M_{h,\beta_2}^{-1}. \tag{5.1}$$

These expressions will allow us to describe the spectrum as a function of the wavenumber k without resorting to numerical computations. In case that the shift is included by adding the term $\gamma\,Q_{h,H}$ to obtain $\widehat{P}_{h,H,\gamma}$ defined by (4.12), the zero eigenvalue of $\widehat{B}_{h,H,\beta_2}$ is shifted to γ without significantly changing the non-zero spectrum. For the variant that uses $\hat{\widehat{E}}_H$, we will revert to a numerical evaluation of the eigenvalues of the deflated preconditioned operator denoted by $\hat{\widehat{B}}_{h,H,\beta_2}$. In the case that the shift parameter γ is zero, this operator is defined by

$$\hat{\widehat{B}}_{h,H,\beta_2} = \hat{\widehat{P}}_{h,H}\,\widehat{A}_h = \hat{\widehat{P}}_{h,H}\,A_h\,M_{h,\beta_2}^{-1}. \tag{5.2}$$

We will consider both the case of zero and non-zero γ. The goal of our analysis is two-fold. We show that the use of First Precondition, Then Deflate method that employs $\widehat{E}_H$ results in a spectrum of clustered eigenvalues favorable for the convergence of a Krylov iteration. We next show that the variant that uses $\hat{\widehat{E}}_H$ results in a spectrum that is remarkably close to the spectrum resulting from the First Deflate, Then Precondition method.

We perform a two-grid Fourier analysis (see e.g. [37]) of $\widehat{B}_{h,H,\beta_2}$ and $\hat{\widehat{B}}_{h,H,\beta_2}$ for a one-dimensional constant wave number problem on the domain $\Omega = (0,1)$. We will use Dirichlet boundary conditions because with these boundary conditions the eigenvalues and eigenvectors of A_h can be determined as described in Section 2. The Fourier analysis that takes the boundary conditions explicitly into account is referred to as rigorous Fourier analysis to distinguish it from a local Fourier analysis.

The fine grid is assumed uniform with meshwidth $h = 1/n$ where $n = 2^p$ and the coarse one is obtained using standard coarsening. With elimination of the boundary conditions, the size of the fine grid operators is $n-1$. Intergrid transfer will be performed by linear interpolation and its transpose. We assume that the preconditioner M_{h,β_2} and the coarse grid operator $\widehat{E}_H$ and $\hat{\widehat{E}}_H$ to be inverted exactly. In a rigorous Fourier analysis the eigenvalues of $\widehat{B}_{h,H,\beta_2}$ are computed by computing the action of $\widehat{B}_{h,H,\beta_2}$ on the eigenvectors of A_h. The latter are the discrete sine functions. The coarse grid aliasing in fact is such that $\widehat{B}_{h,H,\beta_2}$ is found to be similar to a block diagonal matrix with 2×2 diagonal blocks. This implies that we can write

$$\widehat{B}_{h,H,\beta_2} \sim \operatorname{diag}\left[\widehat{B}^{\ell}_{h,H,\beta_2}\right]_{1\le\ell\le n/2} \tag{5.3}$$

where for $1 \le \ell \le n/2-1$, $\widehat{B}^{\ell}_{h,H,\beta_2}$ are the 2×2 matrices and where $\widehat{B}^{n/2}_{h,H,\beta_2}$ is a scalar. The eigenvalues of $\widehat{B}_{h,H,\beta_2}$ can then be computed as the eigenvalues of the diagonal blocks (and similarly for $\hat{\widehat{B}}_{h,H,\beta_2}$). A determining factor in the eigenvalue distribution of $\widehat{B}_{h,H,\beta_2}$ and $\hat{\widehat{B}}_{h,H,\beta_2}$ is the near-kernel of $\widehat{E}_H$ and $\hat{\widehat{E}}_H$, respectively. This motivates looking into these near-kernel first.

We will denote as before $c_\ell = \cos(\ell\pi h)$ and $\kappa = kh$. In our analysis we will use $\beta_2 = 1$ and $\kappa = 0.625$ unless stated otherwise. Motivating the value for $\beta_2 = 1$ is the observation in [29] that in the First Deflate, Then Precondition method the complex shift can be large without compromising the convergence of the outer Krylov acceleration. We assume here that the same argument holds for the First Precondition, Then Deflate method.

5.1. Spectral analysis of Galerkin coarse grid operators

The analysis in [29] can easily be extended to compute the eigenvalues of the Galerkin coarse grid operators $\widehat{E}_H$ and $\hat{\widehat{E}}_H$. For $1 \le \ell \le n/2-1$, this results in

$$\lambda^{\ell}(\widehat{E}_H) = \left(\tfrac{1}{4}(1+c_\ell)^2 \quad \tfrac{1}{4}(1-c_\ell)^2\right)\begin{pmatrix} \frac{2-2c_l-\kappa^2}{2-2c_l-(1+\iota\beta_2)\kappa^2} \\ \frac{2+2c_l-\kappa^2}{2+2c_l-(1+\iota\beta_2)\kappa^2}\end{pmatrix}, \tag{5.4}$$

and

$$\lambda^{\ell}(\hat{\widehat{E}}_H) = \frac{2(1-c_\ell^2)-\kappa^2(1+c_\ell^2)}{2(1-c_\ell^2)-(1+\iota\beta_2)\kappa^2(1+c_\ell^2)}, \tag{5.5}$$

respectively. For $\ell = n/2$ we have that

$$\lambda^{n/2}(\widehat{E}_H) = (2-\kappa^2)/[2-(1+\iota\beta_2)\kappa^2] = \lambda^{n/2}(\hat{\widehat{E}}_H). \tag{5.6}$$

In Fig. 4 we plotted the non-zero eigenvalues of $\widehat{E}_H$ (left) and $\hat{\widehat{E}}_H$ (right) for $k = 100$ using 10 grid points per wavelength in the complex plane. This figure clearly shows that the approximation made to render the construction of $\widehat{E}_H$ computationally feasible and to obtain $\hat{\widehat{E}}_H$ has a negative impact on the eigenvalue distribution. Indeed, Fig. 4 clearly shows that $\hat{\widehat{E}}_H$ has an eigenvalue smaller in size than $\widehat{E}_H$. At large wave numbers, the near-null space of $\hat{\widehat{E}}_H$ will contain more elements than that of $\widehat{E}_H$. This richer near-null space will adversely affect on the eigenvalue distribution of the deflated preconditioned operator $\hat{\widehat{B}}_{h,H,\beta_2}$.

5.2. Deflated preconditioned operator defined using $\widehat{E}_H$

The deflation operator defined by the First Precondition, Then Deflate method using $\widehat{E}_H$ is a projection. The deflated preconditioned operator $\widehat{B}_{h,H,\beta_2} = \widehat{P}_{h,H}\,\widehat{A}_h$ defined by (5.2) without the shift with $\gamma Q_{h,H}$ in $\widehat{P}_{h,H}$ for this method has thus

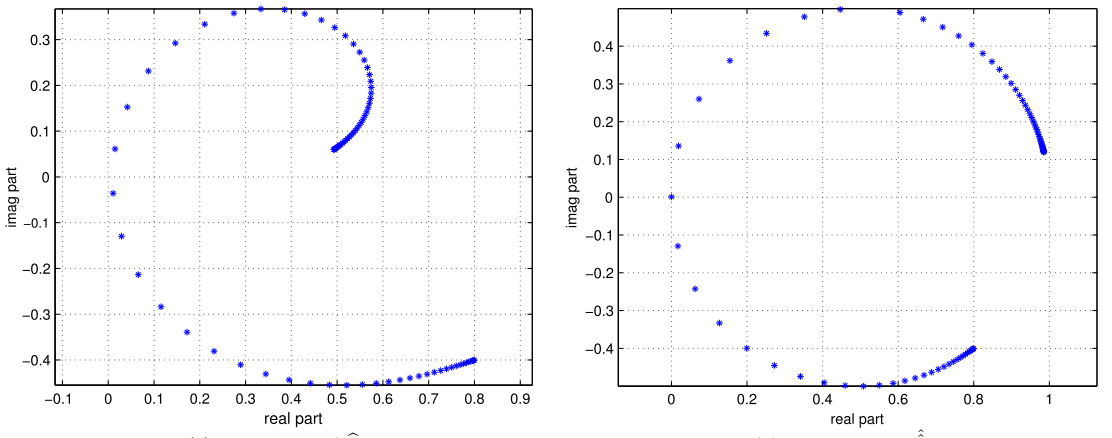

(a) Eigenvalues of $\widehat{E}_H$ (b) Eigenvalues of $\hat{\widehat{E}}_H$

Fig. 4. Eigenvalues of Galerkin coarsened CSLP preconditioned Helmholtz operators $\widehat{E}_H$ (left) and of its approximation $\hat{\widehat{E}}_H$ (right) for $k = 100$ using 10 grid points per wave length.

a zero eigenvalue. A rigorous Fourier analysis yields that this zero eigenvalues has multiplicity $n/2-1$, that $\widehat{B}_{h,H,\beta_2}$ has an eigenvalue equal to $(2-\kappa^2)/(2-\kappa^2(1-\iota\beta_2))$ and additional $n/2-1$ eigenvalues that for $\ell = 1,\ldots,n/2-1$ are of the form

$$\lambda^\ell\big(\widehat{B}_{h,H,\beta_2}\big) = \frac{\widehat{D}(c_\ell,\kappa^2)}{\widehat{F}(c_\ell,\kappa^2) + \iota\,\beta_2\,\widehat{G}(c_\ell,\kappa^2,\beta_2)}\,, \tag{5.7}$$

where the damping parameter β_2 only appears in the imaginary part of the denominator and where $\widehat{D}$, $\widehat{F}$ and $\widehat{G}$ are second order polynomials in κ^2 given by

$$\begin{aligned}
\widehat{D}(c_\ell,\kappa^2) &= (1+c_\ell^2)\kappa^4 - 4(1+c_\ell^2)\kappa^2 + 4(1-c_\ell^4) \\
\widehat{F}(c_\ell,\kappa^2) &= -(1+c_\ell^2)\kappa^4 + 2(2-c_\ell^2+3\,c_\ell^2)\kappa^2 - 4(1-c_\ell^4) \\
\widehat{G}(c_\ell,\kappa^2) &= (1-c_\ell^2)\kappa^4 - 2(1-c_\ell^2)\kappa^4\,.
\end{aligned} \tag{5.8}$$

To understand to what extend this spectrum is clustered and bounded away from the origin, we consider the real and imaginary part of the non-zero eigenvalues that we denote by $\mathrm{Re}\big[\lambda^\ell\big(\widehat{B}_{h,H,\beta_2}\big)\big]$ and $\mathrm{Im}\big[\lambda^\ell\big(\widehat{B}_{h,H,\beta_2}\big)\big]$, respectively. We have that for $\ell = 1,\ldots,n/2-1$

$$\mathrm{Re}\big[\lambda^\ell\big(\widehat{B}_{h,H,\beta_2}\big)\big] = \frac{p(c_\ell,\kappa^2)}{p(c_\ell,\kappa^2) + \beta_2^2\,q(c_\ell,\kappa^2)\,\kappa^4} \tag{5.9}$$

$$\mathrm{Im}\big[\lambda^\ell\big(\widehat{B}_{h,H,\beta_2}\big)\big] = \frac{\beta_2\,r(c_\ell,\kappa^2)\,\kappa^2}{p(c_\ell,\kappa^2) + \beta_2^2\,q(c_\ell,\kappa^2)\,\kappa^4}\,, \tag{5.10}$$

where $p(c_\ell,\kappa^2)$, $q(c_\ell,\kappa^2)$ and $r(c_\ell,\kappa^2)$ are polynomials in κ^2 given by

$$\begin{aligned}
p(c_\ell,\kappa^2) &= (c_\ell^2+1)^2\left[\kappa^8 - 8\kappa^6 - 8(c_\ell-3)\kappa^4 + 32(c_\ell-1)\kappa^2 + 16(c_\ell^2-1)^2\right] \\
q(c_\ell,\kappa^2) &= (c_\ell^2+1)^2\kappa^4 + 4(c_\ell^4-1)\kappa^2 + 4(c_\ell^2-1)^2 \\
r(c_\ell,\kappa^2) &= \kappa^6(1+c_\ell^2)^2 - 2\kappa^4(1+c_\ell^2)(3+c_\ell^2) + 4\kappa^4(1-c_\ell^2)(c_\ell^4+4c_\ell^2+3) - 8(1-c_\ell^2)(1-c_\ell^4)\,.
\end{aligned}$$

The numerator and denominator of $\mathrm{Re}\big[\lambda^\ell\big(\widehat{B}_{h,H,\beta_2}\big)\big]$ are seen to be equal up to the small perturbation $\beta_2^2\,q(c_\ell,\kappa^2)\,\kappa^4$. One can thus expect that $\mathrm{Re}\big[\lambda^\ell\big(\widehat{B}_{h,H,\beta_2}\big)\big] \approx 1$ for $\ell = 1,\ldots,n/2-1$ unless possibly for some value of ℓ we have that $p(c_\ell,\kappa^2) = 0$. Given that the numerator of $\mathrm{Im}\big[\lambda^\ell\big(\widehat{B}_{h,H,\beta_2}\big)\big]$ is small, the analysis yields a tight cluster of non-zero eigenvalues around $(1,0)$ in the complex plane.

In [20] the spectrum of $\widehat{B}_{h,H,\beta_2}$ for $\beta_2 = 0.5$ is computed numerically and plotted in the complex plane. In Fig. 5 instead we plotted using a solid line the real part of these eigenvalues vs. the index ℓ for two values of the wave number k, namely $k = 100$ and $k = 10{,}000$. We used 10 grid points per wavelength and a logarithmic scale on the y-axis. We also plotted using dashed line the real part of the eigenvalues of CSLP preconditioned operator $\mathrm{Re}\big[\lambda^\ell\big(M_{h,1}^{-1}\,A_h\big)\big]$. Plotting both spectra clearly illustrates the action of the deflation operator on the spectrum of the CSLP preconditioned operator. The figure shows that the deflation operator clusters the real part of the eigenvalues around one. This clustering is however not uniform in the wave number. At very high wave numbers the real part of the eigenvalues that correspond to the near-kernel

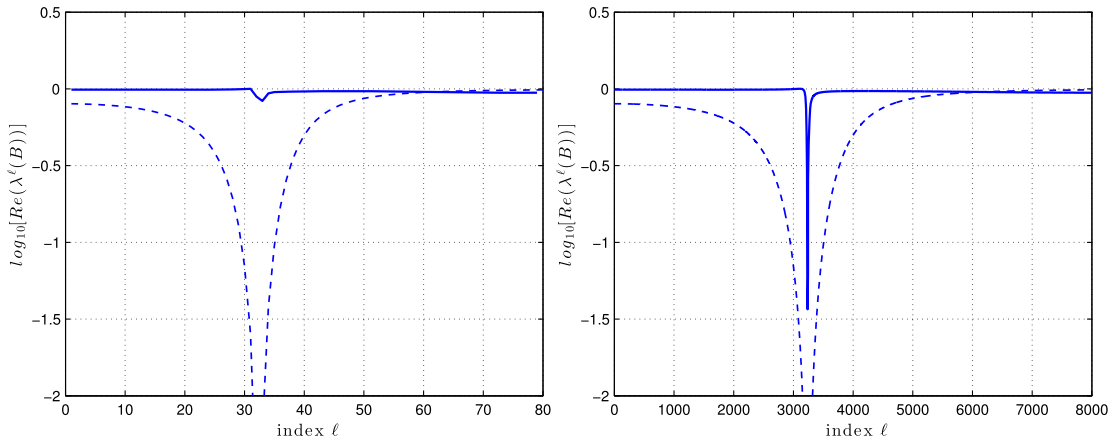

(a) $k = 100$ (b) $k = 10,000$

Fig. 5. Log_{10} of the real part of the non-zero eigenvalues of the deflated preconditioned operator $\widehat{B}_{h,H,1}$ using $\widehat{E}_H$ defined by the First Precondition, Then Deflate method (solid line) and of the preconditioned operator $M^{-1}_{\beta_1,\beta_2} A_h$ (dashed line) with Dirichlet boundary conditions for $k = 100$ and $k = 10{,}000$ using 10 grid points per wave length. The shift towards 0 of the eigenvalues corresponding to the near kernel can clearly be seen.

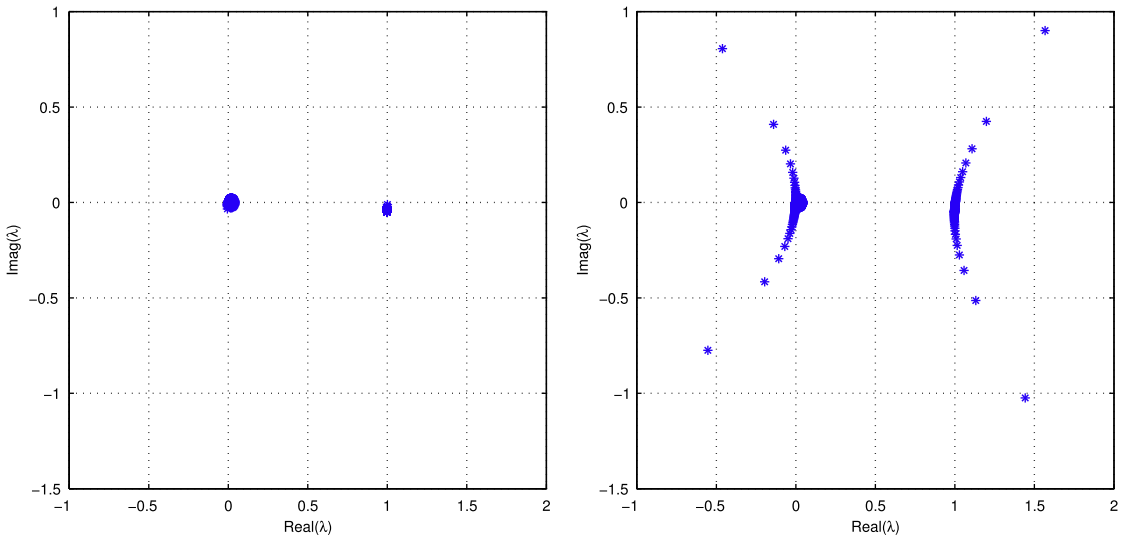

(a) $k = 100$ (b) $k = 10,000$

Fig. 6. Spectrum of the deflated preconditioned operator $\hat{\widehat{B}}_{h,H,1}$ using $\hat{\widehat{E}}_H$ defined by the First Precondition, Then Deflate method assuming no shift (i.e. $\gamma = 0$) with Dirichlet boundary conditions for $k = 100$ and $k = 10{,}000$ using 10 grid points per wave length.

of the Helmholtz equation again moves towards the zero. In the complex plane these eigenvalues thus move towards the origin. The number of eigenvalues undergoing this shift is however much smaller that in the case of merely using CSLP preconditioning.

5.3. *Deflated preconditioned operator defined using* $\hat{\widehat{E}}_H$

The First Precondition, Then Deflate method using the Galerkin coarse grid operator $\hat{\widehat{E}}_H$ defines a deflated preconditioned operator $\hat{\widehat{B}}_{h,H,\beta_2}$ defined by (5.2) that is not a projection. To illustrate to what extent this affects the spectrum of this operator, we will analyze both the case without shift (i.e. setting $\gamma = 0$ in (4.12)) and with shift to one (i.e. setting $\gamma = 1$). The spectrum of $\hat{\widehat{B}}_{h,H,\beta_2}$ without shift and with shift to one is shown in Fig. 6 and Fig. 7, respectively.

Fig. 6 shows the spectrum of $\hat{\widehat{B}}_{h,H,\beta_2}$ for $\beta_2 = 1$ without shift (i.e. $\gamma = 0$) in the complex plane for two values of the wave number k. This figure shows that the zero eigenvalue of multiplicity $n/2 - 1$ of the deflated preconditioned operator $\widehat{B}_{h,H,\beta_2}$ considered in the previous subsection is replaced by a set of small eigenvalues. This figure also shows that the spectrum consists of two clusters, the first around the origin and the second around $(1, 0)$. The spread of both clusters is

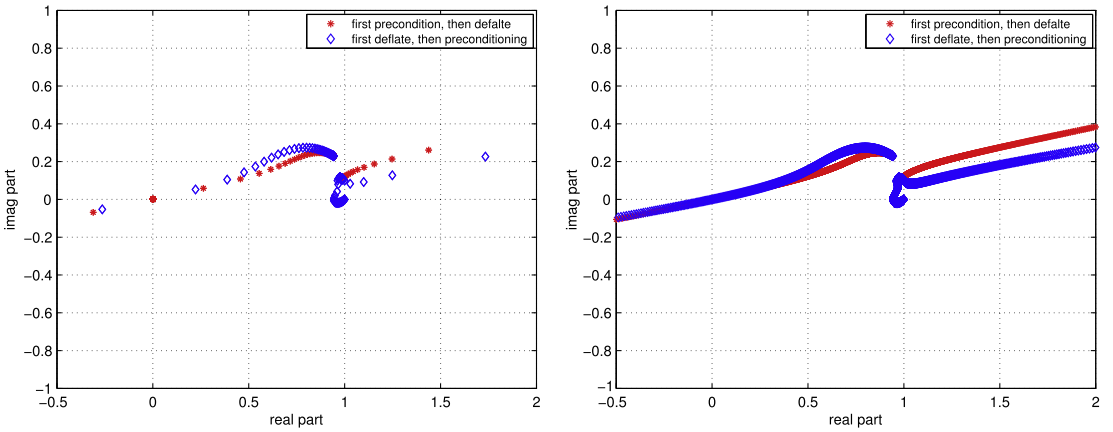

(a) $k = 100$ (b) $k = 10,000$

Fig. 7. Spectrum of two operators. The first is the deflated preconditioned operator $\hat{\hat{B}}_{h,H,1}$ using $\hat{\hat{E}}_H$ defined by the First Precondition, Then Deflate method assuming again shift to one. The second is the preconditioned deflated operator $B_{h,H,1}$ defined by the First Deflate, Then Precondition method assuming shift (i.e. $\gamma = 1$). For both Dirichlet boundary conditions, $k = 100$ and $k = 10{,}000$ and 10 grid points per wave length were used.

seen to grow with the wave number k. For $k = 10{,}000$ in particular the real part of the eigenvalues is bounded below by -1 and above by 2. The imaginary part of these eigenvalues is bounded below by -1 and above by 1.

Fig. 7 shows the spectrum of two operators in the complex plane for two values of the wave number k. The first is the operator $\hat{\hat{B}}_{h,H,\beta_2}$ with shift to one (i.e. $\gamma = 1$) and $\beta_2 = 1$. The second is the preconditioned deflated operator B_{h,H,β_2} defined by (4.14) with again $\gamma = 1$ and $\beta_2 = 1$. The spectrum of the latter was extensively analyzed in [29]. We restricted the range of the real part of the operator to lie between -0.5 and 2. The figure shows a close resemblance. This resemblance is to a large extent caused by the shift, the fact that $\hat{\hat{B}}_{h,H,\beta_2}$ is not a projection and the near-kernel of the Galerkin coarse grid operator. The spectrum is clustered around $(0, 1)$ for low and intermediate wave number values. The spectrum smears out in both directions along the real axis as the wave number increases. Explaining the fact that both spectra closely resemble each other requires further study.

6. Model problem analysis of first deflate, then precondition

In this section we analyze the First Deflate, Then Precondition method introduced in Section 4. We complement the analysis previously published in [29] with new and key insight that the spectrum consists of two sets of eigenvalues. The first set is a tight cluster of eigenvalues that result from the use of deflation. The second set can be further subdivided into two tails that spread away from the cluster in opposite directions along the real axis. This spreading is caused by the near-null kernel components of the Helmholtz coarse grid operator. For a fixed value of κ, the length of the tails and the number of elements in the tail increase proportionally with the wavenumber. The number of eigenvalues not belonging to the cluster however remains small compared to the problem size. The spectrum is therefore favorable to the convergence of the outer Krylov acceleration.

To quantify the claims made on the spectrum, we will in this section first derive closed-form expressions for the eigenvalues of the H^2-scaled Galerkin coarsened Helmholtz operator $H^2 E_H$ and the h^2-scaled deflated preconditioned operator $h^2 P_{h,H} A_h$ defined by (4.2) and (4.4), respectively. We will subsequently discuss the spectrum of the deflated operator $P_{h,H,\gamma} A_h$ with $\gamma = 1$ where the deflation operator includes the shift with $\gamma\, Q_{h,H}$ and of the preconditioned deflated operator $M^{-1}_{h,\beta_2} P_{h,H} A_h$.

6.1. Spectral analysis of Galerkin coarse grid operator

The eigenvalues of the H^2-scaled Galerkin coarsened Helmholtz operator $H^2 E_H$ are for $1 \le \ell \le n/2 - 1$ given by [29]

$$\lambda^{\ell}(H^2 E_H) = 4 - 2(2 + \kappa^2)c_{\ell}^2 - 2\kappa^2\,, \tag{6.1}$$

where $H = 2h$ denotes as before the coarse mesh size. For $\ell = n/2$, we have that $\lambda^{n/2}(H^2 E_H) = 4 - 2\kappa^2$. In the range $1 \le \ell \le n/2 - 1$, the eigenvalues (6.1) increase monotonically between

$$\lambda^{1}(H^2 E_H) \approx -4\kappa^2 < 0 \text{ and } \lambda^{n/2-1}(H^2 E_H) \approx 4 - 2\kappa^2 > 0\,, \tag{6.2}$$

where $c_{\ell=1} \approx 1$ and $c_{\ell=n/2-1} \approx 0$, respectively. The expression (6.1) allows to determine the smallest in size eigenvalue of $H^2 E_H$ and the number of eigenvalues in the near-kernel of this matrix. In analogy with the analysis of the scaled fine

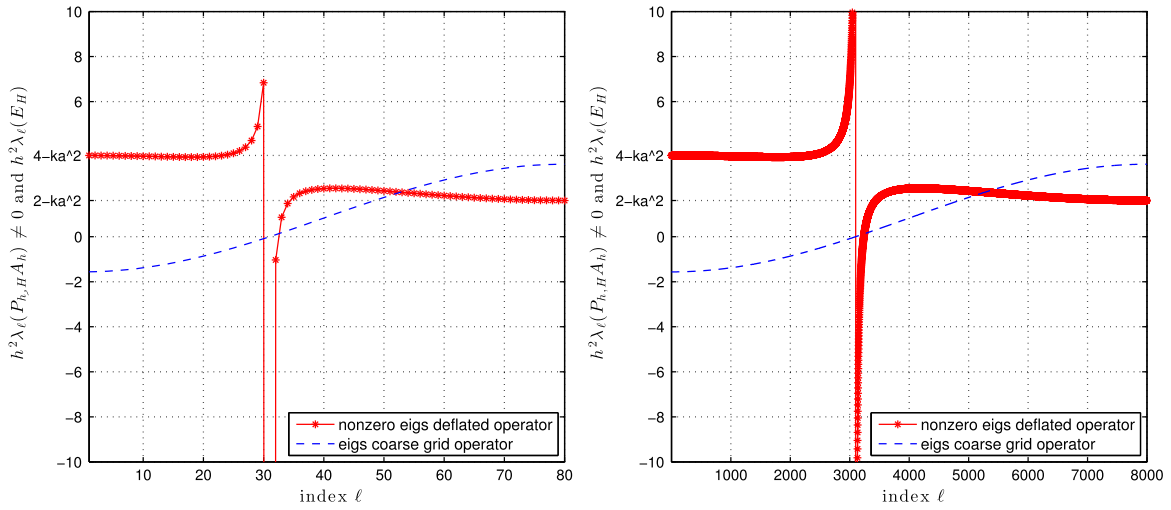

Fig. 8. Eigenvalues of the deflated operator $P_{h,H}\,A_h$ vs. the index ℓ with Dirichlet boundary conditions for $k = 100$ and $k = 10{,}000$ using 10 grid points per wave length. Here the method used is the First Deflate, Then Precondition (A-DEF1) method.

grid Helmholtz operator $h^2 A_h$ in Section 2 we infer that in the limit that k increases for a fixed value of κ, the smallest eigenvalues of $H^2\,E_H$ decreases in size and that the number of eigenvalues in the near-kernel of $H^2\,E_H$ increases. As κ decreases for a fixed value of k, the number of elements in the near-kernel of $H^2\,E_H$ decreases and the corresponding eigenmodes become more low frequent.

6.2. Spectral analysis of the deflated Helmholtz operator

The spectrum of the h^2-scaled deflated Helmholtz operator $h^2\,P_{h,H}\,A_h$ consists of a zero eigenvalue of multiplicity $n/2-1$ and a set of $n/2$ real-valued eigenvalues. For $\ell = n/2$, we have that $\lambda^{n/2}(h^2\,P_{h,H}\,A_h) = h^2$. For $1 \leq \ell \leq n/2-1$ instead we have that

$$\lambda^\ell\left(h^2\,P_{h,H}\,A_h\right) = 2\frac{\left(\mathrm{c}_\ell{}^2+1\right)\kappa^4 + \left(-4\,\mathrm{c}_\ell{}^2-4\right)\kappa^2 - 4\left(\mathrm{c}_\ell{}^4-1\right)}{\lambda^\ell(H^2 E_H)}, \tag{6.3}$$

where the denominator is given by (6.1). Given that for those values of ℓ that corresponds to the near-kernel of $H^2\,E_H$, the numerator is finite and the denominator very small, the eigenvalues $\lambda^\ell\left(h^2\,P_{h,H}\,A_h\right)$ become very large for those values of ℓ. On the extremities of the domain in ℓ instead, we have that

$$\lambda^1\left(h^2\,P_{h,H}\,A_h\right) \approx 4-\kappa^2 \text{ and } \lambda^{n/2-1}\left(h^2\,P_{h,H}\,A_h\right) \approx 2-\kappa^2 \tag{6.4}$$

where $c_{\ell=1} \approx 1$ and $c_{\ell=n/2-1} \approx 0$, respectively.

In Fig. 8 we plotted both the non-zero eigenvalues $\lambda^\ell\left(h^2\,P_{h,H}\,A_h\right)$ as well as the eigenvalues $\lambda^\ell\left(H^2\,E_H\right)$ versus the index ℓ in the range $1 \leq \ell \leq n/2-1$ for $k = 100$ and $k = 10{,}000$ using 10 grid points per wavelength. This figures shows that most of the eigenvalues $\lambda^\ell\left(h^2\,P_{h,H}\,A_h\right)$ lie between $2-\kappa^2$ and $4-\kappa^2$. Eigenvalues not in this range correspond to those values of ℓ in the near-kernel of $H^2\,E_H$ and have both negative and positive values.

The non-zero eigenvalues of $h^2\,P_{h,H}\,A_h$ can thus be partitioned into two sets. The majority of the eigenvalues lies on the real axis between $2-\kappa^2$ and $4-\kappa^2$. A smaller set of eigenvalues can be further subdivided into two tails that develop on both sides of this interval. As k increases for a fixed value of κ, the number of elements in the tail and the length of the tail increases. As κ decreases for a fixed value of k, the number of elements in the tail relative to the problem size decreases.

Computations using a multilevel hierarchy with more than two levels require to include a shift and to add the term $\gamma\,Q_{h,H}$ to $P_{h,H}$ to obtain $P_{h,H,\gamma}$ defined by (4.12). By including this term, the zero eigenvalue of $P_{h,H}\,A_h$ (without shift) is transformed in an eigenvalue γ with the same multiplicity of $P_{h,H,\gamma}\,A_h$ (with shift). The non-zero eigenvalues of $P_{h,H}\,A_h$ are not changed. To obtain a good clustering of the eigenvalues of the CSLP preconditioned operator $M_{h,\beta_2}^{-1}\,A_h$, the value of γ is set equal to 1 as this value is an upper bound for the magnitude of the eigenvalues of the preconditioned operator.

6.3. Spectral analysis of the preconditioned deflated Helmholtz operator

The action of the inverse of the CSLP preconditioner M_{h,β_2}^{-1} is to scale and rotate the non-zero eigenvalues of $P_{h,H,\gamma}\,A_h$ with shift $\gamma = 1$. Plots of the resulting spectrum of $M_{h,\beta_2}^{-1}\,P_{h,H,\gamma}\,A_h$ are given in [29]. Here we are able to give a more

Table 1
Solve time and number of iterations of CSLP/Bi-CGSTAB and A-DEF1 + CSLP/FGMRES(20) for the three-dimensional constant wave number problem using 10 grid points per wave length (Problem 1).

Wave number k	Solve time		Iterations	
	CSLP	A-DEF1 + CSLP	CSLP	A-DEF1 + CSLP
5	0.007	0.055	7	9
10	0.06	0.46	9	10
20	1.07	3.2	21	11
40	21.79	31.99	58	16
60	113.19	165.2	90	23
80	511.80	501.9	159	29
120	2832.7	2056.7	254	39

Table 2
Solve time and number of iterations of CSLP/Bi-CGSTAB and A-DEF1 + CSLP/FGMRES(20) for the three-dimensional constant wave number problem using 20 grid points per wave length (Problem 1).

Wave number k	Solve time		Iterations	
	CSLP	A-DEF1 + CSLP	CSLP	A-DEF1 + CSLP
5	0.04	0.32	7	8
10	0.48	2.32	9	9
20	8.14	17.28	20	9
40	228.29	155.52	70	10
60	1079.99	607.45	97	11

refined interpretation of these plots. The plots in [29] show that the preconditioner does well in clustering those eigenvalues of $h^2 P_{h,H,\gamma} A_h$ that lie in the interval from $2-\kappa^2$ to $4-\kappa^2$. The preconditioner is however not able to cluster the eigenvalues in the earlier described tails of the spectrum of $h^2 P_{h,H,\gamma} A_h$. Therefore two rotated and scaled tails appear in the spectrum of $M_{h,\beta_2}^{-1} P_{h,H,\gamma} A_h$. The preconditioner is unable to repair the shift away from the cluster caused by the near-kernel components of the coarse grid solve. The number of elements in the tails is however small compared to the problem size. The spectrum of $M_{h,\beta_2}^{-1} P_{h,H,\gamma} A_h$ is therefore more favorable to the convergence of an outer Krylov iteration than the spectrum of $M_{h,\beta_2}^{-1} A_h$. Numerical evidence for this statement will be given in the next section.

7. Numerical results

In this section we will demonstrate the performance of the First Deflate, Then Precondition or A-DEF1 Method using the three test problems introduced in Section 2. For preliminary results in which the First Deflate, Then Precondition and the First Precondition, Then Deflate methods are compared, we refer to [38]. Here we focus on the computational efficiency of the first method. We will do so by comparing this method with merely using CSLP as a preconditioner. The first and second solution strategy will be used in combination with FGMRES(20) and Bi-CGSTAB, respectively. We will compare the performance in terms of the required number of outer Krylov iterations and CPU-time. Doing so we will quantify by what amount the use of a coarse grid correction technique is able to accelerate the CSLP preconditioner. Each of the three problems will be discretized by a fine mesh with a number of grid points that allows standard coarsening in each coordinate direction up to obtaining a coarse mesh consisting of a single grid point. In our solver of choice, the combination of A-DEF1 and CSLP is employed recursively to solve the coarser grid problem. This requires the action of CSLP and a flexible Krylov acceleration on each level. On each level we approximate the CSLP preconditioner using one F-cycle with one pre and one post ω-Jacobi ($\omega = 2/3$) smoothing iterations. We will use the shift $\beta_2 = 1$ and $\beta_2 = 5$ when using CSLP with and without deflation, respectively. Motivating this choice is the fact that the previous paper [29] showed that deflation allows for more complex damping without penalizing the convergence of the outer Krylov acceleration. Outer Krylov iterations are started with a zero initial guess and stopped if the scaled residual $\frac{\|r^n\|}{\|b\|}$ is reduced by a factor of 10^7. The number of FGMRES iterations on the second, third and higher coarser levels is set equal to eight, two and one, respectively. Experiments are performed in the PETSc software [30] on a Dell Precision Machine with processor E8400 at 3.00 GHz.

7.1. Three dimensional constant wave number problem

Numerical results for the constant wave number problem (Problem 1 in Section 2) using 10 and 20 grid points per wave length are given in Table 1 and Table 2, respectively. These tables list the number of outer Krylov iterations and CPU-time for various values of the wave number. The solve time reported excludes the time required for the computation of the Galerkin products in the set-up phase of the two algorithms. This set-up time is equal for both algorithms. From these tables it is clear that the use of A-DEF1 results in a reduction in the number of iterations. The reduction in iteration count increases with the wave number. Table 1 in particular shows that without the coarse correction the number of iterations

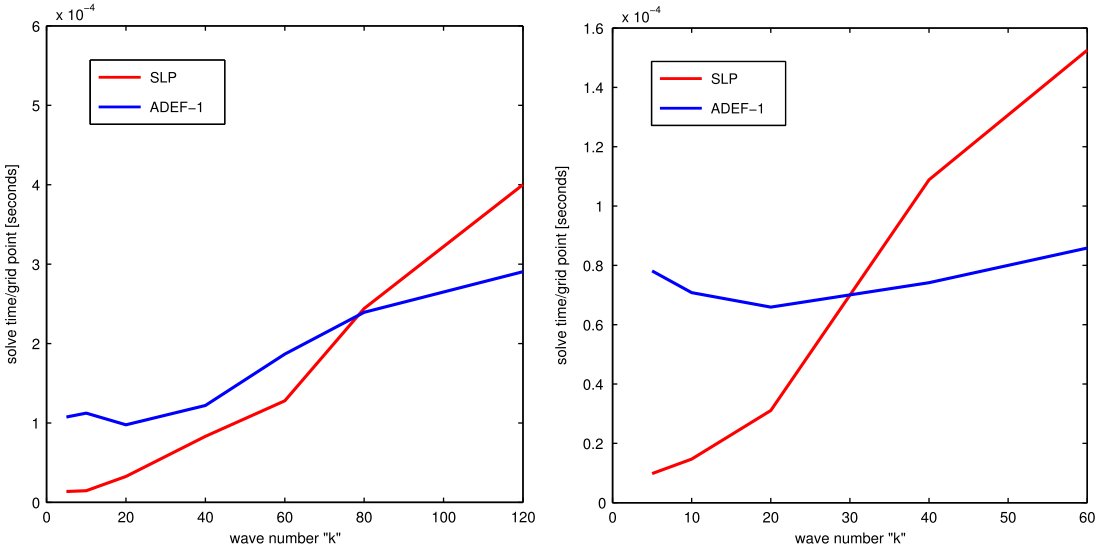

Fig. 9. CPU time per grid point in constant wave number problem using 10 (left) and 20 (right) grid points per wave number (Problem 1).

Table 3
Solve time and number of iterations of CSLP/Bi-CGSTAB and A-DEF1 + CSLP/FGMRES(20) for the three-dimensional non-constant wave number problem using 10 grid points per wave length (Problem 2).

Wave number k	Solve time		Iterations	
	CSLP	A-DEF1 + CSLP	CSLP	A-DEF1 + CSLP
5	0.09	0.24	9	11
10	1.07	1.94	15	12
20	16.70	18.89	32	16
30	73.82	78.04	43	21
40	1304.2	214.7	331	24
60	xx	989.5	xx	34

increases more than linearly with the wave number. With the coarse grid correction this increase is slower than linear. The CPU-time in this table shows a cross-over point between $k = 60$ and $k = 80$. The use of a coarse grid correction results in speed-up for sufficiently large wave numbers. For the largest wave number reported, the use of the coarse grid correction yields a thirty percent reduction in solve time. Table 2 shows that with 20 grid points per wave length the number of A-DEF1 iterations remains almost constant in the range of wave numbers considered. The A-DEF1 solver outperforms the CSLP solver in CPU-time starting at wave number $k = 40$. For the largest wave number considered, a speed-up of forty percent is reported.

The CPU-time per grid point for both solvers using 10 and 20 grid points per wave length is plotted versus the wave number in the left and right part of Fig. 9, respectively. These figures show how the CPU time using the solver variant with deflation increases at a slower rate and is therefore more attractive to use at a given wave number. This cross over wave number is equal to $k = 80$ and $k = 30$ in case that 10 and 20 grid points per wave length are used, respectively.

7.2. Three dimensional variable wave number problem

Numerical results for the non-constant wave number problem (Problem 2 in Section 2) using 10 and 20 grid point per wave length are given in Table 3 and Table 4, respectively. The layered heterogeneity is reflected in an increase in the required number of outer Krylov iterations of both solvers. The problem for $k = 60$ in particular could not be solved using the CSLP solver. The use of A-DEF1 again results in a reduction of the number of iterations and to lower the increase in number of iterations in case that 10 grid points per wave length are used. The use of A-DEF1 results in a six-fold reduction in CPU-time for $k = 40$ and in a converged solution for $k = 60$. In case that 20 grid points per wave length are used, A-DEF1 renders the iteration count almost constant in the range of wave numbers considered. For the largest wave number $k = 30$, the use of A-DEF1 results in a more than ten-fold reduction in CPU time. These results clearly show that the method proposed works in case that the wave number is non-constant throughout the computational domain.

Table 4
Solve time and number of iterations of CSLP/Bi-CGSTAB and A-DEF1 + CSLP/FGMRES(20) for the three-dimensional non-constant wave number problem using 20 grid points per wave length (Problem 2).

Wave number k	Solve time		Iterations	
	CSLP	A-DEF1 + CSLP	CSLP	A-DEF1 + CSLP
5	0.6	1.4	9	9
10	7.5	10.04	14	9
20	324.1	79.2	72	9
30	3810.90	361.7	285	11

Table 5
Solve time and number of iterations of CSLP/Bi-CGSTAB and A-DEF1 + CSLP/FGMRES(20) for the Marmousi problem using 10 grid points per wave length without damping (Problem 3).

Frequency f	Solve time		Iterations	
	CSLP	A-DEF1 + CSLP	CSLP	A-DEF1 + CSLP
1	1.22	5.07	13	7
10	10.18	9.437	112	13
20	72.16	60.32	189	22
40	550.20	426.79	354	39

Table 6
Solve time and number of iterations of CSLP/Bi-CGSTAB and A-DEF1 + CSLP/FGMRES(20) for the Marmousi problem using 10 grid points per wave length with damping parameter set equal to $\alpha = 0.025$ (Problem 3).

Frequency f	Solve time		Iterations	
	CSLP	A-DEF1 + CSLP	CSLP	A-DEF1 + CSLP
1	1.25	5.06	13	7
10	9.63	9.35	106	13
20	70.45	57.47	181	21
40	522.90	424.74	333	38

Table 7
Solve time and number of iterations of CSLP/Bi-CGSTAB and A-DEF1 + CSLP/FGMRES(20) for the Marmousi problem using 20 grid points per wave length without damping (Problem 3).

Frequency f	Solve time		Iterations	
	CSLP	A-DEF1 + CSLP	CSLP	A-DEF1 + CSLP
1	1.23	5.08	13	7
10	40.01	21.83	106	8
20	280.08	131.30	177	12
40	20232.6	3997.7	340	21

7.3. Marmousi problem

Numerical results for the Marmousi problem (Problem 3 in Section 2) are given in Table 5, Table 6 and Table 7. Table 5 and Table 6 consider the problem using 10 grid points per wave length with damping parameter α in Equation (2.1) set equal to $\alpha = 0$ and $\alpha = 0.025$, respectively. Table 7 considers the problem using 20 grid points per wave length and without damping. Table 5 and Table 7 confirm the earlier observed trend that the use of A-DEF1 lowers the number of iterations and that a reduced iteration count results in speedup in solve time at sufficiently high wave number. Table 6 shows that the inclusion of damping renders the problem easier to solve.

8. Conclusions

We have shown that the convergence of the complex shifted Laplacian preconditioner for the Helmholtz equation can be accelerated by combining it with deflation using multigrid vectors. The lower iteration count results for the problems considered in a reduction of computation time by a factor between four and ten depending on the problem size. Particular problems that were previously too large can now be solved. We performed a one-dimensional model problem analysis of two methods. This analysis shows that the First Deflate, Then Precondition method brings most eigenvalues of the Helmholtz operator in the vicinity of $(1, 0)$ in the complex plane. The eigenvalues not belonging to this cluster form two tails on opposite sides of the cluster. These tails are caused by the near-singularity of the Helmholtz coarse grid operator. The number of elements in these tails and the spread of these tails increases with the wavenumber. The computationally expensive variant of the First Precondition, Then Deflate method produces a tightly clustered spectrum. Only at very high wavenum-

bers the spread of the spectrum can be seen. Here the spread is caused by the shift towards zero of the eigenvalues of the Galerkin coarsened preconditioned operator. The computationally feasible variant of the First Precondition, Then Deflate method on the other hand is characterized by a spectrum that closely resembles the one resulting from the First Deflate, Then Precondition method.

References

[1] F. Ihlenburg, I. Babuška, Finite element solution of the Helmholtz equation with high wave number, part I: the h-version of the FEM, Comput. Math. Appl. 30 (9) (1995) 9–37.
[2] O.G. Ernst, M.J. Gander, Why it is difficult to solve Helmholtz problems with classical iterative methods, in: I.G. Graham, T.Y. Hou, O. Lakkis, R. Scheichl (Eds.), Numerical Analysis of Multiscale Problems, in: Lecture Notes in Computational Science and Engineering, vol. 83, Springer, Berlin, Heidelberg, 2012, pp. 325–363.
[3] A. Brandt, I. Livshits, Wave-ray multigrid method for standing wave equations, Electron. Trans. Numer. Anal. 6 (1997) 162–181.
[4] I. Livshits, A scalable multigrid method for solving indefinite Helmholtz equations with constant wave numbers, Numer. Linear Algebra Appl. 21 (2) (2014) 177–193.
[5] H.C. Elman, O.G. Ernst, D.P. O'Leary, A multigrid method enhanced by Krylov subspace iteration for discrete Helmholtz equations, SIAM J. Sci. Comput. 23 (4) (April 2001) 1291–1315.
[6] B. Engquist, L. Ying, Sweeping preconditioner for the Helmholtz equation: hierarchical matrix representation, Commun. Pure Appl. Math. 64 (5) (2011) 697–735.
[7] A. Vion, C. Geuzaine, Double sweep preconditioner for optimized Schwarz methods applied to the Helmholtz problem, J. Comput. Phys. 266 (2014) 171–190.
[8] L. Conen, V. Dolean, R. Krause, F. Nataf, A coarse space for heterogeneous Helmholtz problems based on the Dirichlet-to-Neumann operator, J. Comput. Appl. Math. 271 (2014) 83–99.
[9] G. Bartsch, C. Wulf, Adaptive multigrid for Helmholtz problems, J. Comput. Acoust. 11 (03) (2003) 341–350.
[10] L.N. Olson, J. Schroder, Smoothed aggregation for Helmholtz problems, Numer. Linear Algebra Appl. 17 (2–3) (2010) 361–386.
[11] M.B. van Gijzen, Y.A. Erlangga, C. Vuik, Spectral analysis of the discrete Helmholtz operator preconditioned with a shifted Laplacian, SIAM J. Sci. Comput. 29 (2007) 1942–1958.
[12] S. Cools, W. Vanroose, Local Fourier analysis of the complex shifted Laplacian preconditioner for Helmholtz problems, Numer. Linear Algebra Appl. 20 (4) (2013) 575–597.
[13] Y.A. Erlangga, C. Vuik, C.W. Oosterlee, On a class of preconditioners for solving the Helmholtz equation, Appl. Numer. Math. 50 (3–4) (2004) 409–425.
[14] M.M.M. Mardochê, Incomplete factorization-based preconditionings for solving the Helmholtz equation, Int. J. Numer. Methods Eng. 50 (2001) 1077–1101.
[15] Y.A. Erlangga, C.W. Oosterlee, C. Vuik, A novel multigrid based preconditioner for heterogeneous Helmholtz problems, SIAM J. Sci. Comput. 27 (2006) 1471–1492.
[16] Y.A. Erlangga, C. Vuik, C.W. Oosterlee, Comparison of multigrid and incomplete LU shifted-Laplace preconditioners for the inhomogeneous Helmholtz equation, Appl. Numer. Math. 56 (2006) 648–666.
[17] B. Reps, W. Vanroose, H. Bin Zubair, On the indefinite Helmholtz equation: complex stretched absorbing boundary layers, iterative analysis, and preconditioning, J. Comput. Phys. 229 (November 2010) 8384–8405.
[18] M. Bollhöfer, M.J. Grote, O. Schenk, Algebraic multilevel preconditioner for the Helmholtz equation in heterogeneous media, SIAM J. Sci. Comput. 31 (2009) 3781–3805.
[19] T. Airaksinen, E. Heikkola, A. Pennanen, J. Toivanen, An algebraic multigrid based shifted-Laplacian preconditioner for the Helmholtz equation, J. Comput. Phys. 226 (2007) 1196–1210.
[20] Y.A. Erlangga, R. Nabben, On a multilevel Krylov method for the Helmholtz equation preconditioned by shifted Laplacian, Electron. Trans. Numer. Anal. 31 (2008) 403–424.
[21] M.J. Gander, I.G. Graham, E.A. Spence, Applying GMRES to the Helmholtz equation with shifted Laplacian preconditioning: what is the largest shift for which wavenumber-independent convergence is guaranteed?, Numer. Math. (2015) 1–48.
[22] J. Zhu, X.W. Ping, R.S. Chen, Z.H. Fan, D.Z. Ding, An incomplete factorization preconditioner based on shifted Laplace operators for FEM analysis of microwave structures, Microw. Opt. Technol. Lett. 52 (2010) 1036–1042.
[23] T. Airaksinen, A. Pennanen, J. Toivanen, A damping preconditioner for time-harmonic wave equations in fluid and elastic material, J. Comput. Phys. 228 (March 2009) 1466–1479.
[24] C.D. Riyanti, A. Kononov, Y.A. Erlangga, C. Vuik, C. Oosterlee, R.E. Plessix, W.A. Mulder, A parallel multigrid-based preconditioner for the 3D heterogeneous high-frequency Helmholtz equation, J. Comput. Phys. 224 (2007) 431–448.
[25] Y.A. Erlangga, Advances in iterative methods and preconditioners for the Helmholtz equation, Arch. Comput. Methods Eng. 15 (2008) 37–66.
[26] C. Vuik, A. Segal, J.A. Meijerink, An efficient preconditioned CG method for the solution of a class of layered problems with extreme contrasts in the coefficients, J. Comput. Phys. 152 (1) (1999) 385–403.
[27] J.M. Tang, R. Nabben, C. Vuik, Y.A. Erlangga, Comparison of two-level preconditioners derived from deflation, domain decomposition and multigrid methods, J. Sci. Comput. 39 (3) (2009) 340–370.
[28] J.M. Tang, Two level preconditioned conjugate gradient methods with applications to bubbly flow problems, PhD thesis, DIAM, TU Delft, 2008.
[29] A.H. Sheikh, D. Lahaye, C. Vuik, On the convergence of shifted Laplace preconditioner combined with multilevel deflation, Numer. Linear Algebra Appl. 20 (4) (2013) 645–662.
[30] S. Balay, J. Brown, K. Buschelman, V. Eijkhout, W.D. Gropp, D. Kaushik, M.G. Knepley, L. Curfman McInnes, B.F. Smith, H. Zhang, PETSc users manual, Technical report ANL-95/11 – revision 3.4, Argonne National Laboratory, 2013.
[31] R.J. Versteeg, G. Grau, The Marmousi experience, in: Proc. EAGE workshop on Practical Aspects of Seismic Data Inversion, Copenhagen, 1990, Eur. Assoc. Explor. Geophysicists, Zeist, 1991.
[32] I.M. Babuska, S.A. Sauter, Is the pollution effect of the FEM avoidable for the Helmholtz equation considering high wave numbers?, SIAM Rev. 42 (3) (2000) 451–484.
[33] Y.A. Erlangga, E. Turkel, Iterative schemes for high order compact discretizations to the exterior Helmholtz equation, Modél. Math. Anal. Numér. 46 (03) (2012) 647–660.
[34] Y.A. Erlangga, A robust and effecient iterative method for numerical solution of the Helmholtz equation, PhD thesis, DIAM, TU Delft, 2005.
[35] Y.A. Erlangga, R. Nabben, Algebraic multilevel Krylov methods, SIAM J. Sci. Comput. 31 (2009) 3417–3437.
[36] Y.A. Erlangga, R. Nabben, Multilevel projection-based nested Krylov iteration for boundary value problems, SIAM J. Sci. Comput. 30 (2008) 1572–1595.
[37] U. Trottenberg, C.W. Oosterlee, A. Schüller, Multigrid, Academic Press, London, 2000.
[38] A.H. Sheikh, Development of the Helmholtz solver based on a shifted Laplace preconditioner and a multilevel deflation technique, PhD thesis, DIAM, TU Delft, 2014.